Quasistationary model for determination of ablation parameters in soft-x-ray-driven low- to medium-Z plasma ablation

T. Endo, H. Shiraga, and Y. Kato
Institute of Laser Engineering, Osaka University, 2-6 Yamada-oka, Suita, Osaka 565, Japan
(Received 2 October 1989; revised manuscript received 16 April 1990)

We present a quasistationary model for soft-x-ray-driven ablation of low- to medium-Z plasmas. In this model, the sonic point density is determined self-consistently with the hydrodynamic conservation laws. When this model is applied to an aluminum plasma created by soft-x-ray irradiation, the calculation results for ablation parameters are in good agreement with the published experimental results obtained in the incident x-ray flux region of 10^{12}–10^{13} W/cm^2. Including the higher x-ray flux region, power-law relations for the ablation parameters, such as the sonic point density, the mass ablation rate, and the ablation pressure, are presented. As an application of this model, the rocket foil acceleration due to soft-x-ray-driven ablation is discussed.

I. INTRODUCTION

Laser-produced plasmas are now available as high-intensity x-ray sources in laboratories.[1–3] Dependence of x-ray generation on the atomic number (Z_A) of the target material was studied in order to clarify the physics of x-ray generation in laser-produced plasmas.[4–6] The interaction between an uv laser and a gold plasma has been extensively investigated due to high x-ray conversion efficiency obtainable in this high-Z material.[7–9] When the x-ray conversion efficiency is high, the soft-x-ray radiation generated within the plasma affects its hydrodynamic motion. This effect was studied analytically using the radiation diffusion approximation in a pioneering work by Marshak.[10] More recently, hydrodynamic simulation codes coupled with radiative energy transport were used to analyze energy transport in laser-produced plasmas.[11–14]

Now that the high-intensity x-ray source is available in a laboratory, it is possible to study directly the interaction of intense x-ray radiation with high-density plasmas. Nozaki and Nishihara[15] published a model for deflagration sustained by external soft-x-ray radiation. They classified the soft-x-ray-driven deflagration into two types, supercritical deflagration and subcritical deflagration. In the supercritical deflagration, the radiation energy flux is in thermal equilibrium with the plasma at the Chapman-Jouguet point. That is, the equilibrium thermal radiation sustains the deflagration. In the subcritical deflagration, the radiation energy flux at the Chapman-Jouguet point is not in thermal equilibrium with the plasma. The deflagration is sustained in this case not by the equilibrium thermal radiation, but mainly by the incident radiation. For the supercritical deflagration, Pakula and Sigel[16] published a self-similar model for plasma expansion and radiative energy transport. Their model is based on nonlinear heat conduction using the radiation diffusion approximation. Therefore it is applicable to the case when the blow-off plasma is opaque to the incident radiation, for example, a gold plasma. Behavior of the x-ray-heated gold plasma has been studied experimentally using laser-heated gold cavities.[17–19] The self-similar ablative heat wave model by Pakula and Sigel[16] was applied to these experimental results and was found to be in good agreement not only qualitatively but also quantitatively.[20]

When low- to medium-Z plasmas are heated up to approximately 100 eV by x-ray irradiation and allowed to expand into vacuum, they become quasitransparent to the incident x-ray radiation due mainly to ionization. The importance of the ionization on the spectral opacity was first emphasized in 1983 by Duston *et al.*,[11] who have analyzed radiation transport in aluminum (Al) plasma using a detailed radiation-hydrodynamic model. This ionization burnthrough was experimentally confirmed by Mochizuki *et al.*[21] The radiation field in the quasitransparent plasma is strongly anisotropic. Therefore in the case of low- to medium-Z plasmas, soft-x-ray driven deflagration is subcritical. Accordingly, it cannot be analyzed with a model based on the radiation diffusion approximation which assumes weak anisotropy in the radiation field. For the subcritical deflagration, Nishihara[22] and Yabe *et al.*[23] derived scaling laws using a self-regulating flow model. Their models[22,23] are in qualitative agreement with the experimental results.[24] However, these models are not applicable for quantitatively predicting or analyzing experimental results because the ionic charge state of the x-ray-heated plasma is left as an undetermined parameter. In the subcritical case, the deflagration is sustained mainly by the incident radiation transmitted through the blow-off plasma. In this case, the ionic charge state of the blow-off plasma is an important parameter because it strongly influences the transmission characteristic to the incident radiation.[11,21] Hence it is necessary to determine the ionic charge state of the blow-off plasma self-consistently with other physical quantities.

Recently, Kaiser, Meyer-ter-Vehn, and Sigel published a general analytical model for the x-ray-driven self-similar ablative heating wave.[25] The ablative heating wave corresponds to the subcritical deflagration. Their model assumes that the plasma is fully ionized and the in-

cident x ray is monochromatic. Therefore their model is not always applicable to more realistic cases, for example, when the aluminum is partially ionized due to irradiation by soft x rays of broad spectral bandwidth.

In this paper we describe a calculational model for soft-x-ray-driven ablation in a subcritical limit. The subcritical limit means that the net radiation flux at the Chapman-Jouguet (sonic) point is assumed to consist of only the incident radiation transmitted through the blow-off plasma. The objective of this model is to predict quantitatively the ablation parameters in soft-x-ray-driven ablation in low- to medium-Z materials over a wide x-ray flux region without resorting to complex computer simulations. For this objective, we restrict the atomic numbers of the ablator materials to within 18, and use a few empirical expressions for the atomic data. In Sec. II our calculational model is presented. In Sec. III actual procedures for numerical calculations of the opacity are described. The calculational results are compared with the published experimental results in Sec. IV. In Sec. V scaling laws for the ablation parameters in soft-x-ray-driven ablation are given. In Sec. VI the rocket foil acceleration due to soft-x-ray-driven ablation is discussed. A summary of this work is given in Sec. VII. In the Appendix, the validities of several assumptions made in this work are discussed.

II. QUASISTATIONARY MODEL FOR DETERMINATION OF SONIC POINT DENSITY AND ABLATION PARAMETERS IN SOFT-X-RAY-DRIVEN ABLATION

A schematic diagram of the plasma ablation is shown in Fig. 1. We consider quasistationary deflagration in a reference frame moving with the ablation front. The ablation front is defined as the point at which the density begins to decrease as shown in Fig. 1. Quasistationary state means that each physical quantity is varying so slowly with time that the mass, momentum, and energy conservation laws in a stationary state are valid at each moment. The geometry we treat is one-dimensional and planar. The blow-off plasma is treated as self-similar isothermal expansion. A radiation source, which is assumed to emit blackbody radiation,[26] faces an ablator material across a vacuum space. At the radiation source the radiation emissivity is given by σT_R^4, where σ is the Stefan-Boltzmann constant and T_R is the radiation temperature of the radiation source. At the ablator, the incident radiation energy flux (S_x) is reduced to $k\sigma T_R^4$, where k ($0 \le k \le 1$) depends on the geometrical configuration between the radiation source and the ablator. For open geometry $k \ll 1$, but it becomes closer to 1 for a closed geometry as has been studied by Sigel and coworkers.[18–20]

In the subcritical limit, the net radiation energy flux at the sonic point consists of only the incident radiation transmitted through the blow-off plasma. Hence the transmittance to the incident radiation of the blow-off plasma is a key parameter in this model. In the following, we show first that this transmittance can be obtained from two different, independent approaches. Then we

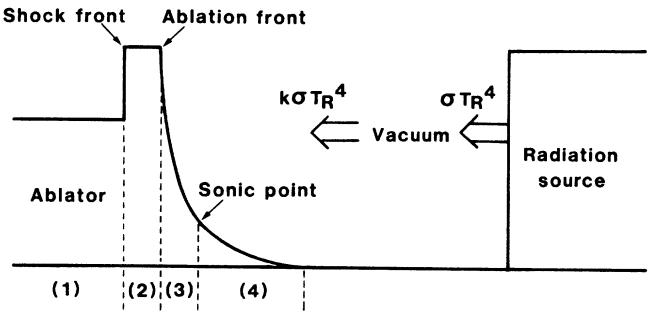

FIG. 1. A schematic diagram of the radiation source and the density profile of the plasma ablation. The regions marked by (1)–(4) correspond to (1) the unperturbed solid region which has infinite thickness, (2) the shock-compressed region, (3) the deflagration region, and (4) the blow-off region.

will show that, by equating these two independent transmittances, the sonic point density (ρ_s) and thus the mass ablation rate and the ablation pressure can be determined uniquely in a self-consistent way.

Two approaches by which we obtain the transmittance to the incident radiation of the blow-off plasma are the following. The first approach is that the transmittance τ_1 is given by the ratio of the energy flux at the sonic point and the energy flux at the plasma-vacuum interface. These fluxes are determined by hydrodynamic conservation laws. The second approach is that the transmittance τ_2 is given by the optical thickness to the incident radiation of the blow-off plasma, which is evaluated by the absorption coefficient of the blow-off plasma and the spectrum of the incident radiation.

The first approach is described in the following. In a quasistationary deflagration, the energy conservation law at each moment is

$$(\rho\varepsilon + P + \tfrac{1}{2}\rho u^2)u + q = \text{const} = Q \ , \tag{1}$$

where ρ is the mass density, ε is the internal energy per unit mass, P is the pressure, u is the fluid velocity in a reference frame moving with the ablation front, q is the total energy flux, and Q is a constant. In more detail, $q = q^e + q^r$, where q^e is the electron thermal energy flux and q^r is the radiation energy flux. The internal energy ε consists of the thermal energy and the energy consumed for ionization. The thermal energy is $\frac{3}{2}(1+z_{\rm av})T$ per ion, where $z_{\rm av}$ is the average ionic charge state and T is the plasma temperature. The energy consumed for ionization is

$$\sum_{m=1}^{Z_A} \sum_{n=0}^{m-1} I(n) f(m)$$

per ion, where Z_A is the atomic number of the ablator material, $I(n)$ is the ionization potential between the ionic charge states n and $n+1$, and $f(m)$ is the fractional population density of the ions with charge state m. We note the relation $P = (n_i + n_e)T = n_i(1+z_{\rm av})T$, where n_i and n_e are the number densities of the ions and the electrons, respectively. Consequently, Eq. (1) is rewritten as

$$\left[\frac{\rho}{m_i}\sum_{m=1}^{Z_A}\sum_{n=0}^{m-1} I(n)f(m)+\tfrac{5}{2}P+\tfrac{1}{2}\rho u^2\right]u+q=Q\ , \quad (2)$$

where m_i is the ion mass.

For simplicity, we assume that the total energy flux q at the ablation front, which represents preheating of the matter ahead of the ablation front, is negligibly small; that is, $q_a=0$, where the subscript a denotes the ablation front. We also assume that the internal energy consumed for ionization at the ablation front is negligibly small.[27] That is,

$$\frac{\rho_a}{m_i}\sum_{m=1}^{Z_A}\sum_{n=0}^{m-1} I(n)f(m)_a=0\ .$$

Based on these assumptions, the constant Q is determined as $Q=(\frac{5}{2}P_a+\frac{1}{2}\rho_a u_a^2)u_a$. Applying Eq. (2) to the sonic point and using the above relation for Q and the mass and momentum conservation laws, the following relation is derived:

$$-q_s=3\rho_s C_s^3 g(\alpha)+S_{\rm ion}\ , \quad (3)$$

where

$$g(\alpha)=1-\tfrac{5}{3}\alpha+\tfrac{2}{3}\alpha^2\ , \quad (4)$$

and

$$S_{\rm ion}=\frac{\rho_s C_s}{m_i}\sum_{m=1}^{Z_A}\sum_{n=0}^{m-1} I(n)f(m)_s\ . \quad (5)$$

The subscript s denotes the sonic point, C is the local sound velocity, and α is the density ratio between the sonic point and the ablation front, that is, $\alpha=\rho_s/\rho_a$. In this model, quasistationary deflagration and following isothermal rarefaction are assumed. That is, the sonic point is at the rear of the quasistationary deflagration region, and beside the front of the isothermal rarefaction region. In this case the gradient of $(1+z_{\rm av})T/m_i$ is negligibly small at the sonic point. Therefore the ratio of specific heats is unity, $\gamma=1$ at the sonic point. Therefore the local sound velocity at the sonic point is given by $C_s=(P_s/\rho_s)^{1/2}$. As to the total energy flux at the sonic point q_s, we assume that the contribution from the electron thermal energy flux is negligible compared with that from the radiation energy flux; that is, $q_s=q_s^r$. This is because the temperature of the x-ray-heated plasma is approximately an order of magnitude lower compared with that of the laser-heated plasma.[28] The validity of this assumption will be discussed in the Appendix.

Since a deflagration wave is subsonic, it works as a piston. Thus the blow-off plasma applies a static pressure and a repulsive force to the matter ahead of the ablation front. As a result, a shock wave is driven ahead of the ablation front.[29] The energy flux required to drive the shock wave is[30]

$$S_{\rm shock}=\rho_s C_s^3(\mu-1)(2-\alpha)\left[\left[\frac{5\alpha(2-\alpha)}{4\mu-1}\right]^{1/2}-\alpha\right]\ , \quad (6)$$

in which $\mu=\rho_a/\rho_0$ where the subscript 0 denotes the unperturbed solid region. Since the blow-off plasma is treated as self-similar isothermal expansion, the energy flux required to maintain the blow-off plasma is given by[30]

$$S_{\rm blow}=4\rho_s C_s^3(1-\tfrac{1}{2}\beta+\tfrac{1}{8}\beta^2)+S_{\rm ion}\ , \quad (7)$$

where $\beta=(\mu-1)[5\alpha(2-\alpha)/(4\mu-1)]^{1/2}+\alpha$. In Eq. (7), we have neglected the spatial variation of the ionization state in the blow-off region, because the drastic changes in temperature and density occur only in the deflagration region. Since deflagration is assumed to be quasistationary, the energy flux required to maintain the whole system is given by

$$\begin{aligned} S_{\rm total}&=S_{\rm shock}+S_{\rm blow}\\ &=4\rho_s C_s^3 h(\mu,\alpha)+S_{\rm ion}\ , \end{aligned} \quad (8)$$

where

$$h(\mu,\alpha)=1-\frac{3\mu^2+8\mu-5}{4(4\mu-1)}\alpha+\frac{3\mu^2+4\mu-4}{8(4\mu-1)}\alpha^2\ . \quad (9)$$

Assuming perfect absorption of the incident x-ray radiation, the x-ray flux incident to the plasma S_x is equated as

$$S_x=S_{\rm total}\ . \quad (10)$$

Therefore the transmittance of the blow-off plasma to the incident x-ray radiation is given by

$$\begin{aligned} \tau_1&=-q_s/S_x\\ &=\frac{3\rho_s C_s^3 g(\alpha)+S_{\rm ion}}{4\rho_s C_s^3 h(\mu,\alpha)+S_{\rm ion}}\ . \end{aligned} \quad (11)$$

From Eq. (10), it is found that S_x is given in terms of density, temperature, and ionic charge state distribution at the sonic point, i.e., $S_x=S_x(\rho_s,T_s,f(m)_s)$. Using a proper ionization model, we can determine $f(m)_s$ as a function of the density and the temperature, that is, $f(m)_s=f(m)_s(\rho_s,T_s)$. Since $S_x=S_x(\rho_s,T_s,f(m)_s)$ and $f(m)_s=f(m)_s(\rho_s,T_s)$, we can uniquely determine $f(m)_s$ and T_s in terms of ρ_s only, when S_x is given and the ablator material is specified. Therefore the transmittance τ_1 is given as a function of ρ_s only.

The second approach to calculate the transmittance of the blow-off plasma to the incident radiation is to evaluate the transmittance as follows:

$$\tau_2=\frac{\int S_\nu\exp(-\tau_\nu)d\nu}{\int S_\nu d\nu}\ , \quad (12)$$

where τ_ν is the optical thickness of the blow-off plasma at the frequency ν, and S_ν is the spectral energy flux of the incident radiation. Equation (12) is valid when radiation is in normal incidence to the ablator surface. When the incident radiation has an angular distribution of $(\cos\theta)^d$, Eq. (12) becomes[31]

$$\tau_2=\frac{\int\left[S_\nu(1+d)\int_1^\infty\frac{\exp(-\tau_\nu w)}{w^{(2+d)}}dw\right]d\nu}{\int S_\nu d\nu}\ . \quad (13)$$

The optical thickness τ_ν is determined by the density and the temperature of the blow-off plasma. Note that we assume the blow-off plasma to be under self-similar isothermal expansion and the variation in the ionic charge state distribution in the blow-off region to be negligible. Then by using a proper ionization model and Eq. (10), the transmittance τ_2 is given also as a function of ρ_s only.

Therefore, for a given ρ_s, two independent values of the transmittance of the blow-off plasma, τ_1 and τ_2, are obtained. Physically τ_1 and τ_2 must be equal. Therefore ρ_s should be self-regulated to the value at which $\tau_1=\tau_2$. Once ρ_s is determined in the procedure mentioned above, the mass ablation rate $\dot{m}$ and the ablation pressure P_a can be determined by the following equations which are derived from the mass and momentum conservation laws:

$$\dot{m}=\rho_s C_s \ , \tag{14}$$

$$P_a=(2-\alpha)\rho_s C_s^2 \ . \tag{15}$$

III. NUMERICAL CALCULATION FOR THE OPACITY OF THE BLOW-OFF PLASMA

In this section we present examples of numerical calculations for the opacity of the blow-off plasma which is required to determine the transmittance τ_2. Several assumptions are made to make the calculations simpler, but without losing the essential aspects of the physics involved. The validities of the assumptions made here are examined in the Appendix.

In the present model, the ionic charge state distribution has to be expressed in terms of the temperature and the density at the sonic point. Here we use a stationary collisional-radiative model by Colombant and Tonon,[32] with the ionization and recombination coefficients given in Ref. 33. An empirical expression for the ionization potential of the multiply charged ions given in Ref. 34 is adopted. Lowering of the ionization potential is neglected, because the blow-off plasma is of relatively high temperature and low density. (See the Appendix for discussion.) Contributions from the excited states and the induced emissions are neglected since the blow-off plasma is of low density. Therefore we treat only the population density of each ionic charge state, not the distribution over the excited states. We assume that the total ion number density is approximately 10^{20} cm^{-3} and the temperature is approximately 100 eV at the sonic point of soft-x-ray-driven ablation. In this case, contribution from the dielectronic-recombination process is negligibly small (less than 10%).[35] Also the photoionization effect on the ionic charge state distribution is neglected in this paper. This effect will be discussed in the Appendix.

The optical thickness τ_ν of the blow-off plasma is determined by considering absorption due to free-free and bound-free transitions. The Kramers formula[31] is used for the absorption coefficient by the free-free transition κ_ν^{ff} as

$$\kappa_\nu^{ff}=\frac{4}{3}\left[\frac{2\pi}{3m_e T}\right]^{1/2}\frac{z_{\rm av}^2 e^6 n_i n_e}{hcm_e\nu^3} \ , \tag{16}$$

where m_e is the electron mass, T is the electron temperature, $z_{\rm av}$ is the average ionic charge state, e is the electron charge, h is the Planck constant, c is the speed of light, ν is the frequency of the x ray, n_i is the ion number density, and n_e is the electron number density. For the absorption cross section by the bound-free transition, we use the following empirical expression, which approximates the tabulated calculation results given in Ref. 36:

$$\begin{aligned}\sigma^{bf}(Z_A,z,h\nu)&=\sigma^K(Z_A,0,E^K(Z_A,0))[E^K(Z_A,0)/h\nu]^3\\&\quad+\sigma^L(Z_A,0,E^L(Z_A,0))[E^L(Z_A,0)/h\nu]^3 \ ,\end{aligned} \tag{17}$$

where superscripts K and L denote the K shell and L shell, respectively, Z_A is the atomic number, z is the ionic charge state, and $h\nu$ is the photon energy which is greater than the absorption edge $E(Z_A,z)$. In Eq. (17)

$$E^K(Z_A,z)=5.62Z_A^{2.19}+12.3z^{1.61}\ ({\rm eV}) \tag{18}$$

and

$$\sigma^K(Z_A,0,E^K(Z_A,0))=2.15\times10^{-16}Z_A^{-2.72}\ ({\rm cm}^2) \tag{19}$$

for the K-shell absorption, and

$$E^L(Z_A,z)=3.69(Z_A-2)^{0.7}(z+1)^{1.3}\ ({\rm eV}) \tag{20}$$

and

$$\sigma^L(Z_A,0,E^L(Z_A,0))=7.41\times10^{-18}Z_A^{2.39}\ ({\rm cm}^2) \tag{21}$$

for the L-shell absorption. When $h\nu$ is less than $E^K(Z_A,z)$ or $E^L(Z_A,z)$, the absorption cross section by the corresponding bound-free transition is zero. These expressions can approximate the tabulated values[36] with the accuracy of better than a factor of 2 for $Z_A\le18$ and $0.1\le h\nu\le4$ keV. Because the M-shell electrons are ionized at $T_e\ge100$ eV in the case of $Z_A\le18$, the bound-free absorption by M-shell electrons can be neglected. The contribution from absorption by bound-bound transitions has been neglected because the spectrally integrated transmittance is not strongly affected by the bound-bound transitions at the density and the temperature mentioned above.[37] The Compton scattering is also neglected because this process does not affect the total absorption coefficient (κ_ν) at the dominant photon energies of the Planckian spectrum of a few hundred eV. The optical thickness τ_ν is thus given by

$$\begin{aligned}\tau_\nu&=n_s C_s t\sum_{z=0}^{Z_A-1}[\sigma^{bf}(Z_A,z,h\nu)f(z)_s]\\&\quad+1.22\times10^{-37}(z_{\rm av}^3 n_s^2 C_s t)/[T_s^{1/2}(h\nu)^3] \ ,\end{aligned} \tag{22}$$

where n_s is the ion number density at the sonic point. In the above formula, T_s and $h\nu$ are in eV, and others are in cgs units.

IV. COMPARISON WITH EXPERIMENTAL RESULTS

We apply the present calculational model to the experiment in which we have measured the velocity of a shock

wave driven by soft-x-ray-driven ablation and evaluated the ablation pressure from the shock wave velocity.[29] The experimental conditions were that the irradiating x-ray flux was 1.9×10^{12} W/cm^2, the x-ray pulse duration was 0.85 ns, and the ablator material was Al. In the calculation, the x-ray irradiation is treated as normal incidence, the treated photon energy range is 0.1–3.0 keV, and other parameters are given in row (a) of Table I. Figure 2 shows the transmittances τ_1 and τ_2 calculated with Eqs. (10)–(12), in terms of the density ratio between the sonic point and the ablation front $\rho_s/\rho_a(=\alpha)$. The closed circle in Fig. 2 shows the solution for the relation $\tau_1=\tau_2$. Once the density ratio α, i.e., ρ_s is determined, other parameters, for example, the mass ablation rate and the ablation pressure, can be determined by Eqs. (14) and (15). The ablation pressure determined by this calculation is 1.2 Mbar, whereas the experimental value was 1.3 Mbar. The calculated ablated depth $\rho_s C_s t/\rho_0$, which corresponds to the amount of the plasma in the blow-off region, is 0.37 μm. The calculational result of the spectral transmittance for this case is shown in Fig. 3. As a reference, the spectral transmittance for the cold (not ionized) Al foil of 0.37-μm thickness is also given together with the Planckian spectrum of 150 eV normalized at its peak value. Figure 3 shows that the photon whose energy is lower than the ionization potential of the ions (absorption edge) in the heated blow-off plasma (approximately 400 eV in this case) passes through the blow-off plasma and deposits its energy to the colder plasma in the deflagration region. That is, the ionization burnthrough plays an important role in the radiation transport, as was shown by Duston *et al.* in Ref. 11.

Furthermore, we make comparison between the model calculation and another experiment where electron temperature was measured spectroscopically as a function of irradiating x-ray flux.[28] The experimental conditions were that the Al plates (50-μm thickness) were irradiated by soft x rays emitted from the laser-produced gold plasma at the x-ray fluxes of 1×10^{12} to 6×10^{12} W/cm^2, with the laser pulse duration of 0.4 ns full width at half maximum (FWHM). In the calculation, the x-ray irradiation is treated as normal incidence, the treated photon energy range is 0.1–3.0 keV, and other parameters are shown in row (b) of Table I. The comparison is shown in Fig. 4, where the experimental results are shown by the vertical bars and the calculation results are given by the solid curve. These comparisons show good agreement between the model calculation and the experimental results, confirming the validity of this calculational model for the parameter ranges given in Table I.

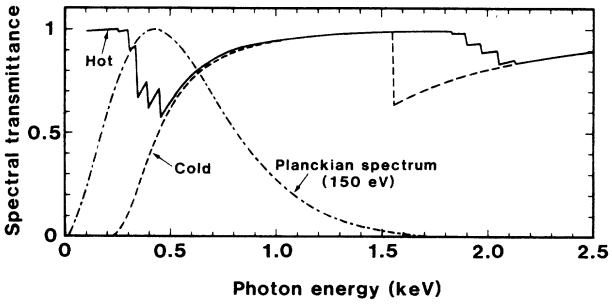

FIG. 3. An example of the calculated spectral transmittance for the hot and cold (not ionized) Al. Planckian spectrum of 150 eV normalized at its peak value is also shown.

V. SCALING LAWS FOR SOFT-X-RAY DRIVEN ABLATION

In this section we present scaling laws for soft-x-ray-driven ablation over broader x-ray flux ranges. Calculation is made for Al which is most frequently used in experiments in fundamental studies of the plasma ablation because of its well-known properties. The calculation was made for the following conditions: the time is 1 ns, the geometrical factor k is unity, the angular distribution of the incident radiation obeys the cosine law with the power of $d=1$, the shock wave is in the strong limit ($\mu=4$), and the treated photon energy range is 0.1–3.0 keV. Figure 5 shows dependences of the important ablation parameters on the x-ray flux, i.e., the temperature T, the sonic point density normalized by the solid density ρ_s/ρ_0, the mass ablation rate $\dot{m}$, and the ablation pressure P_a.

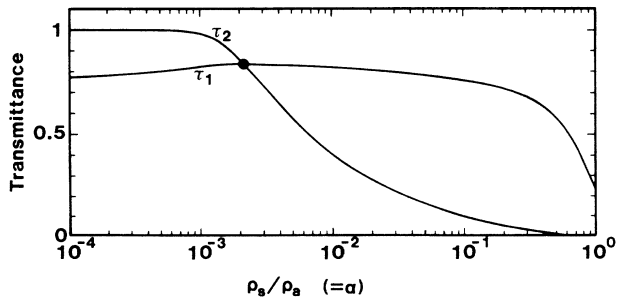

FIG. 2. An example of the calculated transmittances τ_1 and τ_2 in terms of the density ratio ρ_s/ρ_a $(=\alpha)$. The closed circle shows the solution for the relation $\tau_1=\tau_2$, which determines the sonic point density.

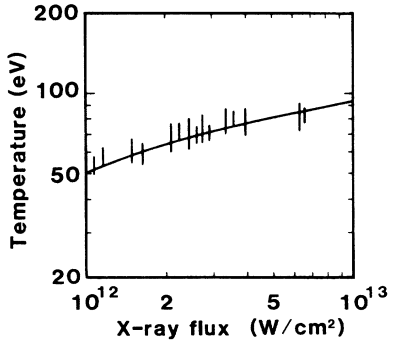

FIG. 4. Comparison between the calculation results (solid curve) and the experimental results given in Ref. 28 (vertical bars) for the electron temperature of the x-ray-heated Al plasma.

TABLE I. Calculation parameters for comparison with the published experimental results.

Ablator material	S_x (W/cm^2)	T_R (eV)	k	Time (ns)	Reference
(a) Al (ρ_0=2.7 g/cm^3, μ=4)	1.9×10^{12}	150	3.8×10^{-2}	0.85	29
(b) Al (ρ_0=2.7 g/cm^3, μ=4)	10^{12}–10^{13}	150	2.0×10^{-2}–2.0×10^{-1}	0.40	28

These dependences can be fitted to power-law relations, especially in the flux region from 3×10^{12} to 3×10^{14} W/cm^2 with good accuracy. This particular flux region is determined by the flux dependence of the ionic charge state distribution, on which the optical thickness of the blow-off plasma depends strongly. Figure 6(a) shows the ionic charge state distribution $f(m)_s$ and the average ionic charge state z_{av} for $t=1$ ns. In Fig. 6(a) we find that, in the flux region mentioned above, the average ionic charge state is $10\le z_{av}\le 11$ and the ionic charge state distribution is relatively simple because the ionization potential of the K-shell electron is much higher than that of the L-shell electrons. This is why the flux dependences of the ablation parameters can be fitted by simple relations.

The ablation parameters depend also on time because the optical thickness of the blow-off plasma is determined not only by the ionic charge state distribution but also by the amount of the ions in the blow-off region. However, the time dependences are relatively weak, and the time dependences can be fitted by simple relations for $0.1\le t\le 10$ *ns*. The power-law relations corresponding to Fig. 5 are as follows:

$$\rho_s/\rho_0 = A_1 S_{13}^{A_2} , \tag{23}$$

$$\dot{m} = A_3 S_{13}^{A_4} \ [\mathrm{g/(cm^2\,s)}] , \tag{24}$$

$$P_a = A_5 S_{13}^{A_6} \ (\mathrm{Mbar}) , \tag{25}$$

where ρ_s/ρ_0 is the sonic point density normalized by the solid density, $\dot{m}$ is the mass ablation rate in g/(cm^2 s), P_a is the ablation pressure in Mbar, S_{13} is the irradiating x-ray flux in 10^{13} W/cm^2, and

$$A_1 = 2.09\times10^{-2} t_{ns}^{-0.250} , \tag{26a}$$

$$A_2 = 0.552 t_{ns}^{-0.037} , \tag{26b}$$

$$A_3 = 3.86\times10^{5} t_{ns}^{-0.154} , \tag{26c}$$

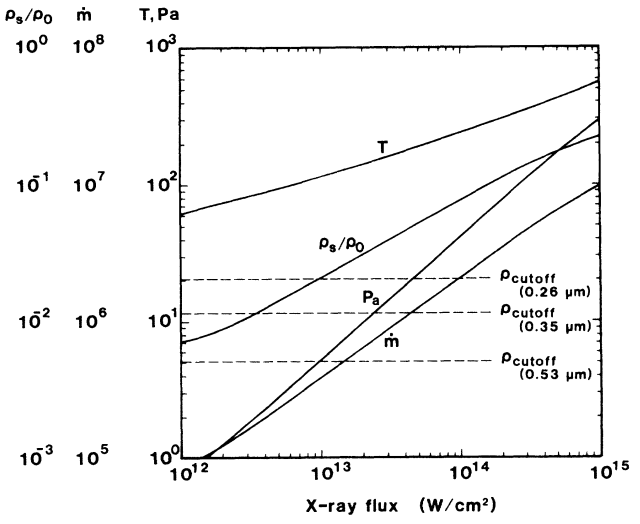

FIG. 5. Calculation results of the ablation parameters in terms of the incident x-ray flux. Here the temperature T is in eV, ρ_s/ρ_0 is the sonic point density normalized by the solid density, the mass ablation rate $\dot{m}$ is in g/(cm^2 s), and the ablation pressure P_a is in Mbar. The curves corresponding to these ablation parameters are labeled by T, ρ_s/ρ_0, $\dot{m}$, and P_a, respectively. Note the difference in the scales in these quantities which are given in the vertical axis. For reference, the cutoff densities to the laser wavelengths of 0.26, 0.35, and 0.53 μm for fully ionized Al plasma normalized by the solid density are also shown by horizontal dashed lines.

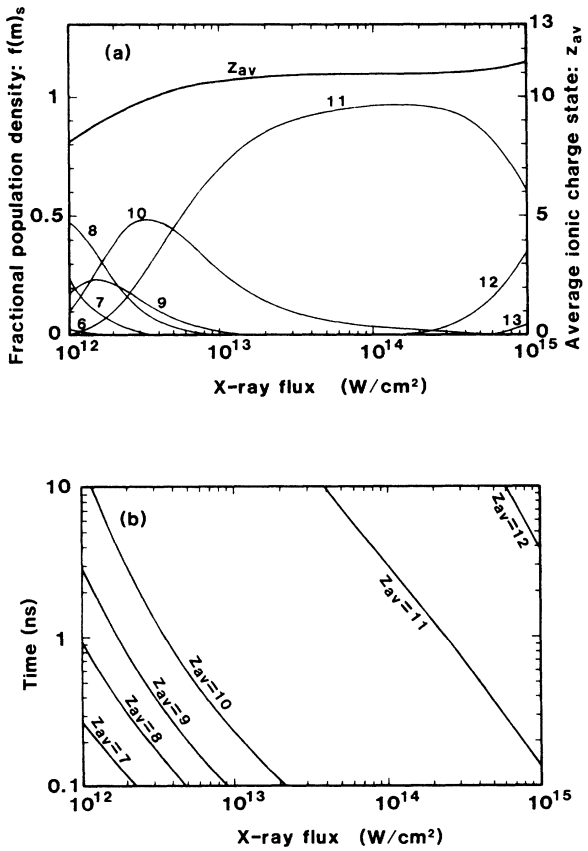

FIG. 6. (a) The average ionic charge state Z_{av} and the fractional population density of each ionic charge state $f(m)_s$ at the sonic point in terms of the incident x-ray flux for the time of 1 ns. The number of each curve refers to the ionic charge state m. (b) Contours of the average ionic charge state in terms of the time and the incident x-ray flux.

$$A_4 = 0.728 t_{ns}^{-0.020} , \tag{26d}$$

$$A_5 = 5.27 t_{ns}^{-0.061} , \tag{26e}$$

$$A_6 = 0.899 t_{ns}^{-0.005} , \tag{26f}$$

where t_{ns} is the time in ns. These power-law relations are applicable for the region of $10 \le z_{av} \le 11$, shown in Fig. 6(b) which shows contours of the average ionic charge state.

VI. ROCKET FOIL ACCELERATION BY SOFT-X-RAY-DRIVEN ABLATION

As an application of the present model, we consider foil acceleration due to soft-x-ray-driven ablation. Compared with laser-driven ablation, the major characteristic of soft-x-ray-driven ablation is that the sonic point density is higher, as shown in Fig. 5, leading to larger mass ablation rate. Therefore the ablated mass before and during acceleration has to be taken into account, when we consider the foil acceleration by soft-x-ray-driven ablation. In the following, we discuss the foil acceleration due to steady-state ablation based on a one-dimensional model. The problem is treated by the steady-state model because time dependences of the ablation parameters are weak and the aim of this discussion is to clarify the major characteristic of soft-x-ray-driven ablation.

We divide the ablative foil acceleration process into two phases: the shock transition phase $0 \le t \le t_1$ and the rocket foil acceleration phase $t_1 \le t \le t_2$. Here $t = 0$ is the onset time of ablation, t_1 is the shock arrival time at the rear surface of the foil, and t_2 is the burnthrough time of the foil. In a laboratory frame, the shock velocity (U_{shock}) and the particle velocity behind the shock front ($U_{particle}$) are given by[30]

$$U_{shock} = \mu \left[\frac{5\alpha(2-\alpha)}{4\mu - 1} \right]^{1/2} C_s , \tag{27}$$

and

$$U_{particle} = (\mu - 1) \left[\frac{5\alpha(2-\alpha)}{4\mu - 1} \right]^{1/2} C_s , \tag{28}$$

respectively. Accordingly, the following relations are obtained:

$$t_1 = \Delta x_0 / U_{shock} = \frac{\Delta x_0}{\mu} \left[\frac{4\mu - 1}{5\alpha(2-\alpha)} \right]^{1/2} \frac{1}{C_s} , \tag{29}$$

$$x(t_1) = 0 , \tag{30}$$

$$v(t_1) = U_{particle} = (\mu - 1) \left[\frac{5\alpha(2-\alpha)}{4\mu - 1} \right]^{1/2} C_s , \tag{31}$$

where Δx_0 is the initial foil thickness, $x(t_1)$ is the position of the foil at t_1, and $v(t_1)$ is the velocity of the foil at t_1.

After the time t_1, the foil is accelerated in accordance with the rocket equation,

$$\frac{dv}{dt} = \frac{P_a}{M_0 - \dot{m} t} , \tag{32}$$

where M_0 is the initial areal mass density of the foil, $M_0 = \rho_0 \Delta x_0$. Integrating the above rocket equation from t_1 to $t\ (< t_2)$ using the initial conditions at t_1, the position of the foil at t is obtained as follows:

$$x(t) = \left[(\mu - 1) \left[\frac{5\alpha(2-\alpha)}{4\mu - 1} \right]^{1/2} + (2 - \alpha) \right] C_s (t - t_1) + (2 - \alpha) C_s (t_2 - t) \ln \left[\frac{t_2 - t}{t_2 - t_1} \right] , \tag{33}$$

where t_2 is given by

$$t_2 = \frac{M_0}{\dot{m}} = \frac{\Delta x_0}{\alpha \mu C_s} . \tag{34}$$

It should be noted that there exists a finite value of $x(t)$ as t approaches t_2. The maximum acceleration distance $x(t = t_2)$ is given by

$$x(t = t_2) = \frac{\Delta x_0}{\alpha \mu} \left[(2 - \alpha\mu) - (4 - \mu) \left[\frac{\alpha(2-\alpha)}{5(4\mu - 1)} \right]^{1/2} \right] . \tag{35}$$

In the strong shock limit $\mu = 4$, the above relation becomes

$$x(t = t_2) = \Delta x_0 \left[\frac{1}{2\alpha} - 1 \right] . \tag{36}$$

where $\Delta x_0 = \dot{m} t_2 / \rho_0$. That is, when the initial foil thickness Δx_0 is given, the maximum acceleration distance $x(t = t_2)$ is determined only by the density ratio between the sonic point and the ablation front.

In laser-driven ablation, the sonic point is considered to be near or below the cutoff density to the incident laser.[38,39] Considering the cutoff point in a fully ionized plasma as the sonic point, the aspect ratio for the one-dimensional (1D) foil acceleration $1/(2\alpha) - 1$ can be evaluated for a given laser wavelength. When the laser wavelength is 0.53 μm and the material is Al, the aspect ratio for the 1D foil acceleration $x(t = t_2)/\Delta x_0$ is evaluated to be about 390. In soft-x-ray-driven ablation, the aspect ratio for the 1D foil acceleration is smaller because of the higher sonic point density. For example, in the case of

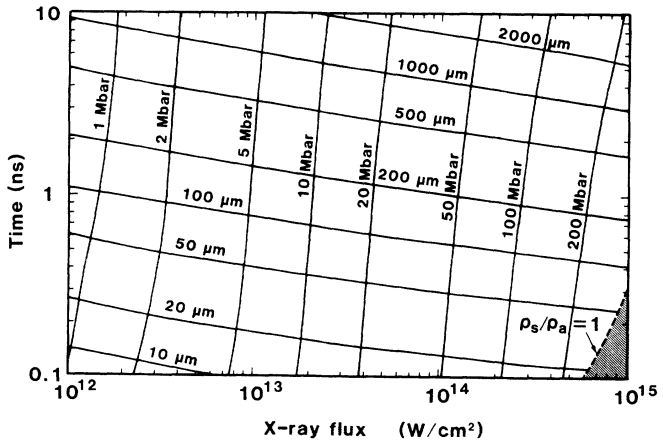

FIG. 7. Contours of the maximum acceleration distance (horizontal curves) and the ablation pressure (vertical curves) in terms of the time and the incident x-ray flux. The hatched area shows the region where the ionization wave is supersonic and deflagration cannot be formed.

$S_x = 10^{14}$ W/cm^2 shown in Fig. 5, $1/(2\alpha)-1=25$ and the maximum acceleration distance is about 200 μm. Figure 7 shows the contours of the maximum acceleration distance and the ablation pressure calculated by our model in terms of the time and the incident x-ray flux. The calculation conditions are the same as Fig. 5 in Sec. V, except for the time.

It should be noted that when the incident x-ray flux is so high that the ionization-wave velocity is higher than the local sound velocity at the ablation front, the ionization wave becomes supersonic and deflagration cannot be formed.[21,22,25] In order to estimate this upper bound of the incident x-ray flux, we calculate the condition where $\rho_s/\rho_a=1$ in the case of the weak shock limit $\mu=1$. The calculation results are also shown in Fig. 7. The right-hand side of the line $\rho_s/\rho_a=1$ in Fig. 7 shows the area where the x-ray flux is too high to form deflagration.[40]

VII. SUMMARY

We presented a calculational model for soft-x-ray-driven ablation of low- to medium-Z plasmas in a quasistationary case. This calculational model was developed essentially based on the ideas of ionization burnthrough by Duston *et al.*[11] and subcritical deflagration by Nozaki and Nishihara.[15] In this model, the energy balances at the plasma-vacuum interface and at the sonic point were considered. The sonic point density was determined uniquely by evaluating the transmittance of the blow-off plasma to the incident radiation. When this model is applied to the Al plasma, the calculation results are in good agreement with the published experimental results in the x-ray flux region of 10^{12}–10^{13} W/cm^2.

For usefulness in designing future experiments, we presented scalling laws for the following ablation parameters: the sonic point density, the mass ablation rate, and the ablation pressure. In order to study the characteristics of soft-x-ray-driven ablation, rocket foil acceleration was discussed. It has been shown that the aspect ratio for the 1D foil acceleration, which is defined as the ratio between the maximum acceleration distance and the initial foil thickness, is determined only by the density ratio between the sonic point and the ablation front. For soft-x-ray-driven ablation, the sonic point density is higher compared with laser-driven ablation, leading to low aspect ratio for the 1D foil acceleration. Finally, the upper bound of the incident x-ray flux was obtained above which the ionization wave becomes supersonic and deflagration cannot be formed.

ACKNOWLEDGMENTS

We thank H. Takabe, K. Mima, and K. Nishihara for valuable discussions. Also we sincerely acknowledge continuous encouragement by Professor S. Nakai and Professor C. Yamanaka. T. Endo received financial support from the Japan Society for the Promotion of Science.

APPENDIX: EXAMINATION OF THE ASSUMPTIONS

In this appendix the validities of the assumptions made in the calculations given in this work are examined. Since it is impossible to examine the validities for all the possible ablator materials, we take Al as a representative example.

1. Quasistationary deflagration

Quasistationary deflagration was assumed at the start of the discussion in Sec. II. As given by Eqs. (23) and (26a), the sonic point density, which is a dominant ablation parameter, scales as $t^{-0.250}$. Because the power of 0.250 is much smaller than unity, the calculation results are consistent with the assumption of the quasistationary deflagration. Since time dependences of the ablation parameters arise mainly from the amount of the blow-off plasma given by $\rho_s C_s t$ $(=\dot{m}t)$, this discussion is applicable when the ablator materials have a similar mass ablation rate to that of Al.

2. Electron thermal energy flux at the sonic point

In the one temperature and stationary model, the electron thermal energy flux is given by $q^e=-\kappa\, dT/dx$, where κ is the electron thermal conductivity which is written as $\kappa=\kappa_0 T^{5/2}$.[41] The temperature gradient is given by

$$\frac{dT}{dx}=\frac{2m_i C_s}{(z_{\rm av}+1)t}\left[1-\frac{\rho_s}{\rho}\right]$$

in the vicinity of the sonic point. Hence the electron thermal energy flux at the sonic point is given by

$$-q_s^e=4.04\times10^6\frac{T^{5/2}m_i C_s}{z_{\rm av}(z_{\rm av}+1)t}\left[1-\frac{\rho_s}{\rho}\right] \tag{A1}$$

where q_s^e is in W/cm^2, T in eV, m_i in amu, C_s in 10^7 cm/s, and t in ns. We evaluate the ratio between the electron thermal energy flux and the radiation energy flux at the sonic point where $1-\rho_s/\rho \ll 1$, as

$$\frac{q_s^e}{q_s^r} \ll \frac{4.04\times 10^6[T^{5/2}m_i C_s]/[z_{\rm av}(z_{\rm av}+1)t]}{\tau_2 S_x} . \quad \text{(A2)}$$

In the region shown in Fig. 6(b), that is, $10^{12} \le S_x \le 10^{15}$ W/cm^2 and $0.1 \le t \le 10$ ns, the maximum value of the right-hand side of (A2) is 0.124, i.e., $q_s^e/q_s^r \ll 0.124$. Therefore at the sonic point, we can neglect the electron thermal energy flux compared with the radiation energy flux.

3. Density effects of the processes neglected in Sec. III

We assumed that the typical values of the total ion number density and the temperature at the sonic point are $n_i = 10^{20}$ cm^{-3} and $T = 100$ eV, respectively. Accordingly the lowering of the ionization potential, the dielectronic-recombination process, and the absorption by bound-bound transitions have been neglected. From the calculation results shown in Fig. 5, typical values of n_i and T can become larger than these values, especially at high x-ray fluxes. Taking $n_i = 5\times 10^{21}$ cm^{-3}, $T = 250$ eV, and $z_{\rm av} = 11$, for $S_x = 10^{14}$ W/cm^2 as the typical parameters, lowering of the ionization potential is estimated to be 62 eV.[42] This value is negligible compared with the ionization potential of 2070 eV for the ions of $z = 11$. Since the parameter region of our interest is close to the case where an ion-sphere model is applicable, ionization potential lowering is proportional to $\rho_s^{1/3}$.[42] At higher x-ray flux, the density ρ_s becomes higher and the potential lowering becomes larger. However, at the same time the ionization potential increases, and thus the ionization potential lowering can be neglected in the region of our interest.

Another effect of increasing the density is to reduce the importance of the dielectronic-recombination process.[43] Hence the assumption of neglecting the dielectronic-recombination process made in Sec. III is valid.

Increase in the density much higher than that assumed in Sec. III has an effect of increasing the absorption by bound-bound transitions. The spectral absorption profiles for the bound-bound transitions are broadened due to the Stark effect.[37] Since the opacity due to the bound-bound transitions is large, profile broadening results in reduced transmittance of the x rays in the blow-off plasma. This leads to reduction in the amount of the ions in the blow-off region and to reduction in the sonic point density ρ_s. The x-ray flux S_x is roughly proportional to $\rho_s C_s^3$. Hence when S_x is fixed, $C_s \sim \rho_s^{-1/3}$. Because the mass ablation rate $\dot{m}$ and the ablation pressure P_a are roughly proportional to $\dot{m} \sim \rho_s C_s$ and $P_a \sim \rho_s C_s^2$, respectively, $\dot{m} \sim \rho_s^{2/3}$ and $P_a \sim \rho_s^{1/3}$. Therefore $\dot{m}$ and P_a calculated by our model will be reduced when the absorption by bound-bound transitions is included.

4. Photoionization effect on the ionic charge state distribution

In the stationary collisional-radiative model including photoionization, the ratio of the ionic population densities between charge states z and $z+1$ is given by

$$\frac{f(z+1)}{f(z)} = \frac{S_c(z)+S_{\rm ph}(z)/n_e}{n_e\alpha_c(z+1)+\alpha_{\rm ph}(z+1)} ,$$

where S_c is the collisional ionization coefficient, $S_{\rm ph}$ is the photoionization coefficient, α_c is the three-body collisional recombination coefficient, $\alpha_{\rm ph}$ is the radiative-recombination coefficient, and n_e is the electron number density. The photoionization coefficient S_{ph} is expressed by

$$S_{\rm ph}(z) = \int \sigma_\nu^{bf}(z)\frac{cU_\nu}{h\nu}d\nu ,$$

where $\sigma_\nu^{bf}(z)$ is the spectral absorption cross section due to bound-free transitions, c is the speed of light, U_ν is the spectral radiant energy density, and $h\nu$ is the photon energy.

The importance of the photoionization depends on the ratio between $S_{\rm ph}(z)/n_e$ and $S_c(z)$. The collisional ionization coefficient $S_c(z)$ is strongly dependent on the ratio between the ionization potential $I(z)$ and the electron temperature T_e, because $S_c(z)$ includes the term $\exp[-I(z)/T_e]$.[33] That is, the photoionization becomes important only when $I(z)/T_e$ is large. In the parameter region of our interest ($10^{12} \le S_x \le 10^{15}$ W/cm^2 and $0.1 \le t \le 10$ ns), the photoionization is not negligible only for the ions which have only K-shell electrons because of its large ionization potential. That is, the photoionization is not negligible in the parameter region of $z_{\rm av} \ge 11$ as is shown in Fig. 6(b).

For estimation of the photoionization effect on the important ablation parameters, ρ_s, $\dot{m}$, P_a, we carried out the calculations including the photoionization in an approximate way. In this calculation, we approximated the spectral radiant energy density as $U_\nu = S_\nu/c$ where S_ν is the incident spectral radiant energy flux. This approximation corresponds to the extremely optically thin plasma case, which is consistent with the subcritical deflagration. The results of this calculation show that the photoionization effects on ρ_s, $\dot{m}$, and P_a are negligible in the parameter region of $10^{12} \le S_x \le 10^{15}$ W/cm^2 and $0.1 \le t \le 10$ ns. The deviation in these parameters is within approximately 10%. This is qualitatively explained as follows. The photoionization promotes ionization and increases the energy consumed for ionization $S_{\rm ion}$. For certain values of density and incident x-ray flux, temperature and ionic charge state distribution must obey the energy conservation law at the plasma-vacuum interface, Eq. (10). Therefore the photoionization leads to larger $S_{\rm ion}$ but also to smaller $\rho_s C_s^3$. As a result, the effect of photoionization to the transmittance τ_1, which is determined by Eq. (11), is not significant. Also the effect of photoionization to the transmittance τ_2, which is determined by Eq. (12), is not significant. This is because the photoionization decreases the absorption due to bound-free transitions, but increases the absorption due to free-free transitions. Consequently, the deviation in the solution for the relation $\tau_1 = \tau_2$ due to photoionization is very small, and the deviations in the important ablation parameters remain negligible.

5. Effects of the x rays emitted in the x-ray-heated plasma

The model described in this work treats soft-x-ray-driven ablation in the subcritical limit, where the net radiation energy flux at the sonic point consists only of the incident x rays transmitted through the blow-off plasma. Actually, the x-ray-heated plasma also emits soft x rays which should influence the ablation behavior. The conversion efficiency from plasma thermal energy to radiation energy depends strongly on the structure of the deflagration region. However, the structure of the deflagration region is beyond the model described here, in which only the energy balances are treated. Therefore we will discuss only the effects of the self-emitted radiation. The radiation energy fluxes at the sonic point and at the plasma-vacuum interface are schematically shown in Fig. 8. At the plasma-vacuum interface, S_x and $\eta_x S_x$ are, respectively, the inward and the outward radiation energy fluxes where η_x is the x-ray reemission efficiency. The net inward radiation energy flux is thus given by $(1-\eta_x)S_x$. At the sonic point, $\tau_2 S_x$ is the incident radiation energy flux transmitted through the blow-off plasma, and S_{SE_1} and S_{SE_2} are the inward and the outward self-emitted radiation energy fluxes, respectively. The net inward radiation energy flux at the sonic point is thus given by $\tau_2 S_x+(S_{\mathrm{SE}_1}-S_{\mathrm{SE}_2})$. Consequently, the energy balance at the sonic point is given by $\tau_2 S_x+(S_{\mathrm{SE}_1}-S_{\mathrm{SE}_2})=\tau_1(1-\eta_x)S_x$. When $|S_{\mathrm{SE}_1}-S_{\mathrm{SE}_2}|\ll\tau_2 S_x$, the subcritical limit approximation is valid and the energy balance at the sonic point is given by $\tau_2=\tau_1(1-\eta_x)$.

We should discuss the case when $|S_{\mathrm{SE}_1}-S_{\mathrm{SE}_2}|$ is not negligible compared with $\tau_2 S_x$. First we discuss the effect of the self-emitted radiation in the case for $S_{\mathrm{SE}_1}\gg S_{\mathrm{SE}_2}$. The subcritical limit and the supercritical limit correspond to the cases of $\tau_2 S_x\gg S_{\mathrm{SE}_1}-S_{\mathrm{SE}_2}$ and $\tau_2 S_x\ll S_{\mathrm{SE}_1}-S_{\mathrm{SE}_2}$, respectively. In the following, we estimate the transition condition from subcritical to supercritical deflagration. Considering that the blow-off plasma is treated as isothermal expansion, the following relation holds:

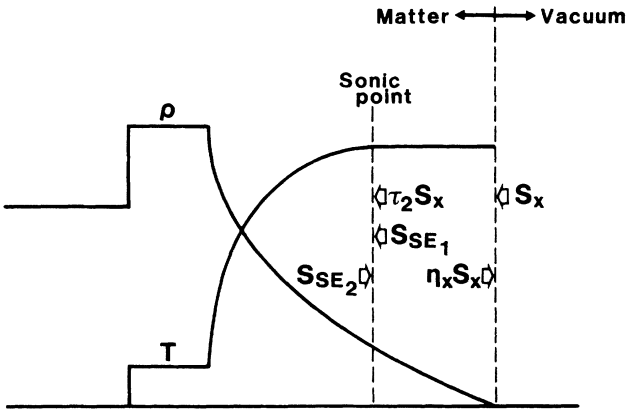

FIG. 8. A schematic diagram of the radiation energy fluxes at the plasma-vacuum interface and at the sonic point.

$$S_{\mathrm{SE}_1}-S_{\mathrm{SE}_2}\approx S_{\mathrm{SE}_1}\leq\eta_x S_x\ . \tag{A3}$$

For supercritical deflagration in which the self-emitted radiation sustains the deflagration , $\tau_1(1-\eta_x)S_x\approx S_{\mathrm{SE}_1}-S_{\mathrm{SE}_2}$. Using $\tau_1\approx\frac{3}{4}$ from Eq. (11), the transition condition from subcritical to supercritical deflagration is given by $\eta_x\geq\frac{3}{7}$.[44] According to the ablative heat wave model,[16,20] which corresponds to the supercritical limit, the x-ray reemission efficiency η_x (which is called reemission coefficient r in Ref. 20) is given for Au by

$$\eta_x=\frac{2.87S_{\mathrm{HW}_{13}}^{3/13}t_{\mathrm{ns}}^{8/13}}{1+2.87S_{\mathrm{HW}_{13}}^{3/13}t_{\mathrm{ns}}^{8/13}}\ , \tag{A4}$$

where $S_{\mathrm{HW}_{13}}=(1-\eta_x)S_x$ is the net energy flux into the matter in 10^{13} W/cm^2. For $S_{\mathrm{HW}}=10^{13}$ W/cm^2 and $t=1$ ns, $\eta_x=0.74$, which is larger than the critical x-ray reemission efficiency of $\frac{3}{7}$. For subcritical deflagration, we have shown in Sec. IV that, in the incident x-ray flux region from 10^{12} to 10^{13} W/cm^2, the calculational results by the present model agree with the published experimental results for Al. However, for the higher x-ray flux region it is necessary to compare the present model calculation with experiments using low- to medium-Z materials. This is because for higher x-ray flux, the temperature of the x-ray-heated plasma becomes higher and the ablated depth becomes larger, thereby increasing η_x.

Next, we discuss the case when $S_{\mathrm{SE}_1}\ll S_{\mathrm{SE}_2}$. In this case, the deflagration is sustained by the incident radiation, and is subcritical. The energy balance at the sonic point is given by $\tau_2 S_x=\tau_1(1-\eta_x)S_x+(S_{\mathrm{SE}_2}-S_{\mathrm{SE}_1})$. However, the ablation behavior is considerably influenced by the self-emitted radiation when the net outward radiation energy flux due to the self-emitted radiation $(S_{\mathrm{SE}_2}-S_{\mathrm{SE}_1})$ becomes comparable with the required energy flux to sustain the hydrodynamic motion $\tau_1(1-\eta_x)S_x$, that is, $(S_{\mathrm{SE}_2}-S_{SE_1})\approx\tau_1(1-\eta_x)S_x$. On the other hand, the following relation holds, since the temperature in the blow-off region is higher than that in the deflagration region:

$$S_{\mathrm{SE}_2}-S_{\mathrm{SE}_1}\approx S_{\mathrm{SE}_2}\leq\eta_x S_x\ . \tag{A5}$$

Accordingly the condition that the self-emitted radiation considerably influence the ablation behavior is given by $\tau_1(1-\eta_x)\leq\eta_x$. Using $\tau_1\approx\frac{3}{4}$, this condition is given by $\eta_x\geq\frac{3}{7}$. The discussion in the second case is applicable to laser-driven ablation, in which soft-x-ray radiation is generated mainly in the deflagration region where plasma is relatively of low temperature and high density.[4,9] Recent experimental studies of laser-driven ablation with uv laser irradiation show that the ablation behavior of an Au foil is considerably different from that of an Al foil.[7,45] The conversion efficiency from the incident uv laser energy to the x-ray energy in Au plasma is higher than 60%, whereas it is about 20% in Al plasma.[3] These experimental results are consistent with the discussion in the case when $S_{\mathrm{SE}_1}\ll S_{\mathrm{SE}_2}$.

[1]H. Nishimura, F. Matsuoka, M. Yagi, K. Yamada, S. Nakai, G. H. McCall, and C. Yamanaka, Phys. Fluids **26**, 1688 (1983).

[2]D. L. Matthews, E. M. Campbell, N. M. Ceglio, G. Hermes, R. Kauffman, L. Koppel, R. Lee, K. Manes, V. Rupert, V. W. Slivinsky, R. Turner, and F. Ze, J. Appl. Phys. **54**, 4260 (1983).

[3]R. Kodama, K. Okada, N. Ikeda, M. Mineo, K. A. Tanaka, T. Mochizuki, and C. Yamanaka, J. Appl. Phys. **59**, 3050 (1986).

[4]T. Mochizuki, T. Yabe, K. Okada, M. Hamada, N. Ikeda, S. Kiyokawa, and C. Yamanaka, Phys. Rev. A **33**, 525 (1986).

[5]P. Alaterre, H. Pépin, R. Fabbro, and B. Faral, Phys. Rev. A **34**, 4184 (1986).

[6]R. Popil, P. D. Gupta, R. Fedosejevs, and A. A. Offenberger, Phys. Rev. A **35**, 3874 (1987).

[7]P. D. Gupta, Y. Y. Tsui, R. Popil, R. Fedosejevs, and A. A. Offenberger, Phys. Rev. A **34**, 4103 (1986).

[8]P. D. Goldstone, S. R. Goldman, W. C. Mead, J. A. Cobble, G. Stradling, R. H. Day A. Hauer, M. C. Richardson, R. S. Marjoribanks, P. A. Jaanimagi, R. L. Keck, F. J. Marshall, W. Seka, O. Barnouin, B. Yaakobi, and S. A. Letzring, Phys. Rev. Lett. **59**, 56 (1987).

[9]W. C. Mead, E. K. Stover, R. L. Kauffman, H. N. Kornblum, and B. F. Lasinski, Phys. Rev. A **38**, 5275 (1988).

[10]R. E. Marshak, Phys. Fluids **1**, 24 (1958).

[11]D. Duston, R. W. Clark, J. Davis, and J. P. Apruzese, Phys. Rev. A **27**, 1441 (1983).

[12]R. F. Schmalz, J. Meyer-ter-Vehn, and R. Ramis, Phys. Rev. A **34**, 2177 (1986).

[13]D. Salzmann, H. Szichman, A. D. Krumbein, and C. E. Capjack, Phys. Fluids **30**, 515 (1987).

[14]R. Marchand, R. Fedosejevs, C. E. Capjack, and Y. T. Lee, Laser Part. Beams **6**, 183 (1988).

[15]K. Nozaki and K. Nishihara, J. Phys. Soc. Jpn. **48**, 993 (1980).

[16]R. Pakula and R. Sigel, Phys. Fluids **28**, 232 (1985).

[17]K. Okada, T. Mochizuki, N. Ikeda, M. Hamada, M. Mineo, R. Kodama, and C. Yamanaka, J. Appl. Phys. **59**, 2332 (1986).

[18]S. Sakabe, R. Sigel, G. D. Tsakiris, I. B. Földes, and P. Herrmann, Phys. Rev. A **38**, 5756 (1988).

[19]G. D. Tsakiris and R. Sigel, Phys. Rev. A **38**, 5769 (1988).

[20]R. Sigel, R. Pakula, S. Sakabe, and G. D. Tsakiris, Phys. Rev. A **38**, 5779 (1988).

[21]T. Mochizuki, K. Mima, N. Ikeda, R. Kodama, H. Shiraga, K. A. Tanaka, and C. Yamanaka, Phys. Rev. A **36**, 3279 (1987).

[22]K. Nishihara, Jpn. J. Appl. Phys. **21**, L571 (1982).

[23]T. Yabe, S. Kiyokawa, T. Mochizuki, S. Sakabe, and C. Yamanaka, Jpn. J. Appl. Phys. **22**, L88 (1983).

[24]T. Mochizuki, S. Sakabe, K. Okada, H. Shiraga, T. Yabe, and C. Yamanaka, Jpn. J. Appl. Phys. **22**, L133 (1983).

[25]N. Kaiser, J. Meyer-ter-Vehn, and R. Sigel, Phys. Fluids B **1**, 1747 (1989).

[26]The model in this paper is applicable to more general cases of non-Planckian spectra. For simplicity, we assume blackbody radiation which is a fairly good approximation to the spectrum of x-ray emission from Au plasmas.

[27]Strictly, there exists pressure ionization by shock compression, while the plasma temperature is low at the ablation front. However, the objective of this paper is not to discuss complicated atomic physics or equations of state in the high-density region. It is to investigate the representative properties of soft-x-ray-driven ablation using a simplified model without resorting to complex computer simulations.

[28]R. Kodama, M. Kado, K. A. Tanaka, A. Yamauchi, T. Mochizuki, T. Yamanaka, S. Nakai, and C. Yamanaka, Phys. Rev. A **37**, 3622 (1988).

[29]T. Endo, H. Shiraga, K. Shihoyama, and Y. Kato, Phys. Rev. Lett. **60**, 1022 (1988).

[30]H. Takabe, K. Nishihara, and T. Taniuti, J. Phys. Soc. Jpn. **45**, 2001 (1978).

[31]Ya. B. Zel'dovich and Yu. P. Raizer, *Physics of Shock Waves and High-Temperature Hydrodynamic Phenomena* (Academic, New York, 1967).

[32]D. Colombant and G. F. Tonon, J. Appl. Phys. **44**, 3524 (1973).

[33]R. K. Landshoff and J. D. Perez, Phys. Rev. A **13**, 1619 (1976).

[34]N. Miyanaga, Ph. D. thesis, Osaka University, 1987. The empirical expression is as follows. For K-shell electrons, $I(z)=13.6Z_A^{0.7}(z+1)^{1.3}$ (eV); for L-shell electrons, $I(z)=3.69(Z_A-2)^{0.7}(z+1)^{1.3}$ (eV); for M-shell electrons, $I(z)=2.81(Z_A-10)^{0.7}(z+1)^{1.3}$ (eV).

[35]D. Salzmann and A. Krumbein, J. Appl. Phys. **49**, 3229 (1978).

[36]R. F. Reilman and S. T. Manson, Astrophys. J. Suppl. Ser. **40**, 815 (1979).

[37]D. Salzmann and G. Wendin, Phys. Rev. A **18**, 2695 (1978).

[38]P. Mora, Phys. Fluids **25**, 1051 (1982).

[39]W. M. Manheimer, D. G. Colombant, and J. H. Gardner, Phys. Fluids **25**, 1644 (1982).

[40]In Ref. 21, this upper bound of the incident x-ray flux was estimated to be 2×10^{13} W/cm^2 for Al, which is much lower than that shown in Fig. 7. The main reason for this difference is the assumption made in Ref. 21 that the plasma temperature is equal to the radiation temperature and that the ionic charge state of the x-ray-heated plasma is determined by the relation $z_{av}^2 I_H = T$, where I_H is the ionization potential of a hydrogen atom. Using their assumption, when $S_x=2\times10^{13}$ W/cm^2, the average ionic charge state becomes only 3, which is much lower than that shown in Fig. 6(b). This leads to underestimation of the required energy flux to sustain the ionization wave, overestimation of the ionization-wave velocity, and consequently underestimation of the upper bound of the incident x-ray flux.

[41]S. I. Braginskii, *Review of Plasma Physics* (Consultants Bureau, New York, 1965), Vol. 1, p. 205.

[42]J. C. Stewart and K. D. Pyatt, Jr., Astrophys. J. **144**, 1203 (1966).

[43]C. De Michelis and M. Mattioli, Nucl. Fusion **21**, 677 (1981).

[44]In Ref. 15, the transition condition is given by $3\rho_s C_s^3=\sigma T_s^4$, which in our case corresponds to $\tau_1(1-\eta_x)S_x=S_{SE_1}$. However, S_{SE_1} is smaller than σT_s^4 due to low opacity in the case of low- to medium-Z materials. Therefore the condition in Ref. 15 will give a rather low transition temperature.

[45]K. A. Tanaka, A. Yamauchi, R. Kodama, T. Mochizuki, T. Yabe, T. Yamanaka, S. Nakai, and C. Yamanaka, J. Appl. Phys. **65**, 5068 (1989).